JACS Au
AN OPEN ACCESS JOURNAL OF THE AMERICAN CHEMICAL SOCIETY

Editors' Choice
Open Access

pubs.acs.org/jacsau
Article

Metal-Independent Correlations for Site-Specific Binding Energies of Relevant Catalytic Intermediates

Shyama Charan Mandal and Frank Abild-Pedersen*

Cite This: JACS Au 2024, 4, 4790−4798
Read Online

ACCESS | Metrics & More | Article Recommendations | Supporting Information

ABSTRACT: Establishing energy correlations among different metals can accelerate the discovery of efficient and cost-effective catalysts for complex reactions. Using a recently introduced coordination-based model, we can predict site-specific metal binding energies (ΔE_M) that can be used as a descriptor for chemical reactions. In this study, we have examined a range of metals including Ag, Au, Co, Cu, Ir, Ni, Os, Pd, Pt, Rh, and Ru and found linear correlations between predicted ΔE_M and adsorption energies of CH and O (ΔE_{CH} and ΔE_O) at various coordination environments for all the considered metals. Interestingly, all the metals correlate with one another under specific surface site coordination, indicating that different metals are interrelated in a particular coordination environment. Furthermore, we have tested and verified for PtPd- and PtIr-based alloys that they follow a similar behavior. Moreover, we have expanded the metal space by taking some early transition metals along with a few s-block metals and shown a cyclic behavior of the adsorbate binding energy (ΔE_A) versus ΔE_M. Therefore, ΔE_{CH} and ΔE_O can be efficiently interpolated between metals, alloys, and intermetallics based on information related to one metal only. This simplifies the process of screening new metal catalyst formulations and their reaction energies.

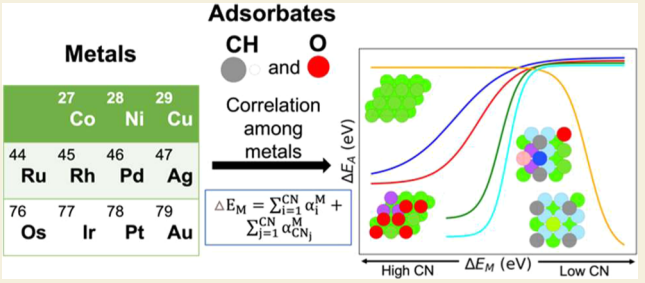

KEYWORDS: *density function theory, coordination-based α-scheme model, binding energies, metal-independent correlation, hydrocarbon-based adsorbates, sigmoid function*

1. INTRODUCTION

Heterogeneous catalysis plays a critical role in advancing sustainability within chemical reactions. Platinum group elements (PGEs) have been extensively utilized for various thermal and electrochemical reactions such as the hydrogen evolution reaction, the oxygen reduction reaction, and hydrocarbon combustion reactions.[1−7] The limited availability of catalysts based on PGE and their high costs pose a barrier to the widespread adoption and use at large scale.[8] In addition, there is still significant room for improvement in the catalytic activity and product selectivity. To overcome these challenges and enhance sustainability in chemical reactions, more cost-effective and efficient catalyst alternatives are needed. In this context, numerous detailed experimental and theoretical studies have shed light on this topic.[9−16] A combination of experimental insight and theoretical investigations is needed to provide a valuable understanding of heterogeneous catalysis. Utilizing density functional theory (DFT) to calculate reaction energies and activation energies, we can rationalize the activity, selectivity, and stability of a catalyst surface. However, the identification of efficient catalysts remains a time-consuming and tedious process since catalysts are dynamic under operation requiring feedback between experimental and theoretical efforts.[17] To speed up the process, recent advancements in machine learning and artificial intelligence have been utilized in catalysis.[18] But these approaches often lack the ability to provide a comprehensive understanding of the fundamental properties of the catalyst and how to link these to observations for fluctuating systems. Hence, it is of utmost importance to develop a comprehensive model which accurately and efficiently combines input based on information about the local structure of the catalyst.[19,20] Such models would not only expedite the catalyst screening process but also provide a solid foundation for understanding catalysis at a fundamental level. In recent years, remarkable advancements have been made in establishing links between adsorption energies.[21−23] Such approaches significantly reduce efforts and screening times for catalysts. Recently, a coordination-based model, known as the α-scheme model, was constructed with the goal to predict the binding energy of an active surface site (ΔE_M) in a diverse coordination environment.[24,25] Armed with

Received: August 20, 2024
Revised: October 8, 2024
Accepted: October 28, 2024
Published: December 5, 2024

this new descriptor, we have successfully demonstrated correlations with adsorption energies of various hydrocarbon-based adsorbates along with CO and OH and efficiently linked a vast number of hydrocarbon-based adsorbates in the simple classification scheme.[22,26] The recent classification of adsorbates was performed specifically on Pt, and in this paper, we aim to expand the framework to include other transition metals. Crucially, all these findings are strongly correlated with the site stability, leading us to introduce a novel descriptor, ΔE_M, for catalysis.

In this study, we have investigated the correlation of various metals on a specific surface site coordination starting from an α-scheme model-predicted ΔE_M (Figure 1). A wide range of

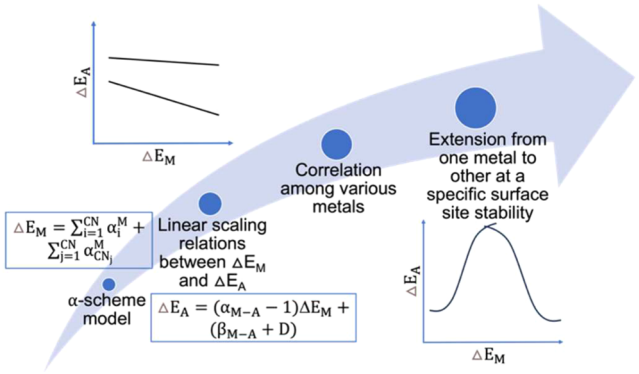

Figure 1. This schematic figure illustrates a step-by-step process for understanding metal binding energies (ΔE_M) and their metal correlation for specific surface site coordination. The coordination-based α-scheme model can predict ΔE_M and shows how the binding energies of adsorbate (ΔE_A) exhibit a linear scaling relationship with ΔE_M. Various metals are correlated with each other for specific surface site coordination.

metals, including Ag, Au, Co, Cu, Ir, Ni, Os, Pd, Pt, Rh, and Ru, were examined, and a statistically significant number of calculations were used to extrapolate the α-parameters for each metal to accurately predict ΔE_M. We have chosen CH and O as relevant intermediates due to their key role in a wide range of hydrocarbon- and steam-based reactions.[21,22,27] We demonstrate strong correlations among all the metals at a specific coordination environment, enabling us to efficiently predict and understand the behavior of different metals in similar coordination environments, contributing to the advancement of catalyst design and optimization for sustainable chemical reactions. We have also tested our model for alloys and found that it follows a behavior similar to that observed for metals. We expanded the screened metal space to include early transition metals as well as s-block metals and as expected we find a periodic behavior of the ΔE_A versus ΔE_M as we gradually empty the atomic orbitals.

2. COMPUTATIONAL DETAILS

The Vienna Ab initio Simulation Package (VASP) was utilized in conjunction with the Atomic Simulation Environment (ASE) to carry out all the first-principles density functional theory (DFT) calculations.[28−31] To incorporate exchange−correlation effects, we have considered the BEEF-vdW functional,[32,33] a well-established method that has been extensively validated for calculating adsorbate binding energies on metal surfaces.[22,34] The plane wave basis sets were employed during optimization were set with a cutoff energy of 500 eV. To ensure accurate results, all structures were optimized until the total energies converged to a minimum of 10^{-5} eV, and the forces reached a threshold of less than 0.05 eV/Å. The metal lattice constants utilized in this study were obtained from earlier reports[22,24,34] or calculated using the equation of state computational approaches. The optimized lattice constants for each metal at face-centered cubic (fcc) lattice are as follows: Ag 4.22, Au 4.20, Co 3.46, Cu 3.68, Ir 3.88, Ni 3.55, Os 3.86, Pd 3.98, Pt 3.98, Rh 3.85, and Ru 3.81 Å. For the binding energy calculations, we employed 7 layers of 3 × 3 M(100) and 3 × 3 M(111), whereas for (211) we have considered 7 layers of 1 × 3 slabs. In all the structures, the bottom four layers were kept fixed, while the remaining layers were allowed to relax during the system optimization process. The considered adsorbates CH and O have been adsorbed on the top site of metals. To mitigate periodic image interactions, a significant vacuum region of more than 15 Å was introduced between the slabs in the z-direction. The Monkhorst Pack method was employed to generate appropriate k-point grids within the Brillouin zone.[35] For the reciprocal space of the surfaces, a 4 × 4 × 1 k-point grid was utilized to solve the DFT-based Kohn−Sham equations. Furthermore, to eliminate any artificial periodic interactions between the slabs, dipole corrections were applied.[36] The gas phase molecules were optimized within a 21 Å × 22 Å × 23 Å cell. A 1 × 1 × 1 k-point density was used during the optimization of the gas phase molecules. To calculate the metal or adsorbate binding energies, we used the following eqs 1a and 1b

$$\Delta E_M = E_{slab+M} - (E_{slab} + E_M) \quad (1a)$$

$$\Delta E_A = E_{slab+A} - (E_{slab} + E_A) \quad (1b)$$

In the above eqs 1a and 1b, ΔE_M and ΔE_A represent the binding energies of the metal and the adsorbate, respectively, E_{slab}, E_{slab+M}, and E_{slab+A} are the calculated total energies of the bare slab, the slab with adsorbed metal (M), and the slab with adsorbate (A), respectively. E_M is the total energy of metal (M), whereas E_A is the total energy of adsorbate (A). All the structures and binding energies can be found in cathub (https://www.catalysis-hub.org/publications/MandalMetal2024).[37]

3. RESULTS AND DISCUSSION

In the following section, we discuss (i) the choice of metals and validation of the α-scheme model, (ii) the correlation of metal binding energies with adsorbate binding energies (ΔE_M vs ΔE_A), (iii) the correlation among different metals and maximum binding energies for specific adsorbates, and finally, we validate our model for alloys and expand it beyond the transition metals to illustrate the periodic behavior of the ΔE_A versus ΔE_M. This helps to establish simple and useful correlations for various metals within specific coordination environments.

3.1. Choice of Metals and Validation of the α-Scheme Model

To establish the necessary correlations, we explored site binding energies, ΔE_M, within a given coordination environment. We have focused on a selection of relevant transition metals, namely Ag, Au, Co, Cu, Ir, Ni, Os, Pd, Pt, Rh, and Ru. These metals have been selected due to their significance in catalytic reactions, rendering them highly relevant to our investigation. Recent studies have extensively utilized most of

https://doi.org/10.1021/jacsau.4c00759
JACS Au 2024, 4, 4790−4798

these metals in a variety of essential reactions. For instance, Ag, Au, Ni, Cu, and Ru are successfully used for dihydrogen bond activation,[38−40] while Pt, Ru, Ni, Co, and Rh have shown promise for C−H bond activation in hydrocarbon chemistry.[41−43] Additionally, Pt is important because of its efficiency in the hydrogen evolution reaction,[7,44] hydrocarbon combustion,[4,45] and oxygen reduction reaction,[46,47] while Ir excels in the oxygen evolution reaction,[48,49] and Cu is recognized for its potential in CO_2 reduction reaction.[50,51] However, to further enhance the catalytic activity and reduce costs, researchers have extensively explored the catalytic activity of cheaper metals and the compositions thereof. Throughout our study, we have placed specific emphasis on analyzing the behavior of these metals within the face-centered cubic (fcc) crystal structure. After carefully considering the selection of metals, we proceeded to evaluate our coordination-based α-scheme model using the BEEF-vdW functional. According to the α-scheme model, the metal binding energies can be predicted from the identity of the metal atom and the changes to the metal coordination number. We identify the energy of a metal atom Z in specific coordination number n as $E_n^Z = \sum_{i=1}^{n} \alpha_i^Z$, and we can evaluate the α_i^Z parameters through a limited set of distinct model surface DFT calculations. For a metal in an fcc crystal structure, knowing the following 12 α_i^Z values α_{1-3}^Z, α_4^Z, α_5^Z,⋯, α_{11}^Z, $\alpha_{12,100}^Z$, $\alpha_{12,111}^Z$, $\alpha_{12,\text{bulk}}^Z$, we can approximate the binding energies of metal atoms in any coordination environment. For convenience, we use $\alpha_{1-3}^Z = \alpha_1^Z + \alpha_2^Z + \alpha_3^Z$, and for increased accuracy, we consider three different α_{12}^Z values for 100, 111 and bulk as they are slightly different even when they have the same coordination number. It is important to note that we only account for nearest-neighbor interactions in the model as the consideration of next-nearest interactions and beyond has very little effect on the metal binding energies. As an example, let us consider a metal atom on a 111 surface with coordination number $n = 3$ then we can estimate the binding energy of the metal atom Z as $\Delta E_M = \alpha_{1-3}^Z + 3\alpha_{10}^Z$ can be represented as the addition of α_{1-3}^Z and three α_{10}^Z. To obtain the α-values, we performed a statistically significant number of DFT calculations (18 binding energy calculations) for each individual metal.[22,24] In this study, the α-values were calculated relative to the bulk energy of the metal atoms, as accurately calculating gas phase energies of these atoms using DFT can be challenging, and we would like to compare the results from one metal to another. Therefore, we chose to use the face-centered cubic (fcc) bulk energy of metal atoms as the reference point during ΔE_M calculations. Whenever we consider the energy of bulk metal atoms as a reference as opposed to the gas phase energy of the metal, we essentially subtract the cohesive energy of the metal from the gas phase energy. Therefore, in all cases, the binding energy of the metal can be represented by the following equation

$$\Delta E_M = E_M^i - E_M^{coh} \tag{2}$$

In the above eq 2, ΔE_M is the binding energy of the considered metal with respect to the bulk energy of that respective metal, E_M^i is the binding energy of the metal atom i with respect to gas phase, and E_M^{coh} is the cohesive energy of the metal. Based on the α-scheme model, the cohesive energy of the system can be derived by summing all the α-values, i.e., $\sum_{i=1}^{12} \alpha_i^M$ for fcc bulk structures. Hence, by combining these two aspects, we can derive the following equation representing ΔE_M concerning the bulk metal as a reference

$$\Delta E_M = \sum_{i=1}^{CN} \alpha_i^M + \sum_{j=1}^{CN} \alpha_{CN_j}^M - \sum_{i=1}^{12} \alpha_i^M \tag{3}$$

Figure 2 illustrates the integral plot of all the α-values for increasing coordination. A complete list of these α-values is

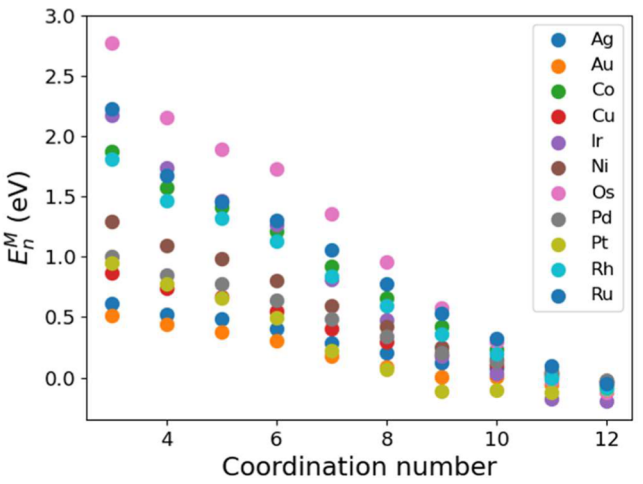

Figure 2. Fcc metal atom energies as a function of their coordination number. The energy values were obtained through calculations using the bond-associated α_i^Z parameters. α_{12}^M is the average value of $\alpha_{12,\text{bulk}}^Z$, $\alpha_{12,100}^Z$, and $\alpha_{12,111}^Z$.

provided in the Supporting Information Table S1. When extracting the α-values using 18 binding energy calculations for each metal, we obtain the following MAE values: Ag: 0.023, Au: 0.041 Co: 0.054, Cu: 0.032, Ir: 0.111, Ni: 0.042, Os: 0.148, Pd: 0.039, Pt: 0.062, Rh: 0.053, and Ru: 0.092 eV. Among all the metals, the highest MAE was observed for Os, 0.148 eV, and the lowest MAE was found for Ag, 0.023 eV. Once determined, these α-parameters can be applied effectively to various structures within the complete set of metals, eliminating the need for redundant calculations in other applications. With this coordination-based model, we are now able to accurately predict the ΔE_M using the α values which directly reflect the coordination environment of the respective metals. The same has been shown in earlier reports.[22,24,26] This simple framework significantly enhances the practicality and applicability of our model, allowing us to make reliable predictions for a wide range of scenarios without the need for repeated computations. The α-scheme model was employed to predict ΔE_M, and a comparison was made with DFT-calculated ΔE_M for all of the metals under consideration. The resulting data are shown in Figure S1 in the Supporting Information. The figures demonstrate good agreement and hence justification for applying the α-scheme model in predicting ΔE_M across all of the metals examined. This level of accuracy in predicting the binding energy through the established model further substantiates the reliability and robustness of our approach.

3.2. Correlation of Metal Binding Energies with Adsorbate Binding Energies (ΔE_M vs ΔE_A)

In agreement with earlier studies, we find that binding energies of hydrocarbon-based adsorbates (ΔE_A) follow a linear correlation with the α-predicted metal binding energies (ΔE_M).[22,26] The linear scaling relationship between the

https://doi.org/10.1021/jacsau.4c00759
JACS Au 2024, 4, 4790−4798

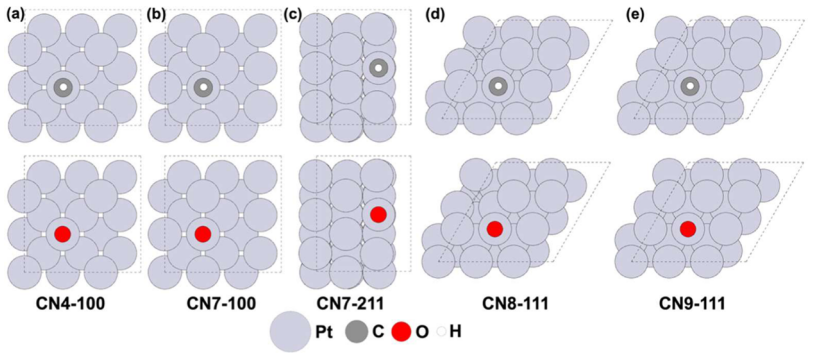

Figure 3. (a–e) Model structures applied to establish the linear correlations between the DFT-calculated ΔE_A (A = CH and O) and the α-predicted ΔE_M. The ΔE_M values with respect to the bulk metal energy values were obtained using bond-associated α_i^Z parameters.

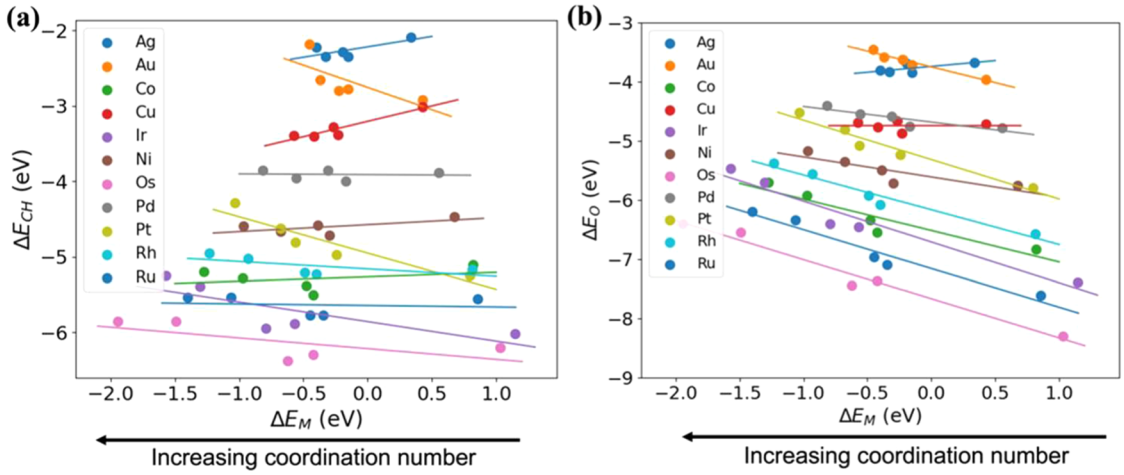

Figure 4. DFT-calculated adsorbate energies ΔE_A have been plotted against the surface site stability ΔE_M predicted using the α-scheme. Site stabilities are referenced to the energy of bulk metal atoms. (a) Shows on top adsorption energies ΔE_{CH} versus ΔE_M adsorption and (b) shows on top adsorption energies ΔE_O versus ΔE_M adsorption.

binding energy of adsorbates and the metal binding energies anticipated by the α-scheme model can be expressed in eq 4

$$\Delta E_A = (\alpha_{M-A} - 1)\Delta E_M + (\beta_{M-A} + D) \quad (4)$$

In eq 4, the coefficient $\alpha_{M-A} - 1$ represents the binding strength of the adsorbates on the catalytic surface, and the two intercept parameters $\beta_{M-A} + D$ are associated with the gas phase complexes. To verify the applicability of the correlation to the considered adsorbate (CH and O) binding energies and the descriptor ΔE_M, a selection of data points was employed, encompassing a range of α-scheme predicted metal binding energies. These points span from low metal coordination (weak metal binding energy) to high metal coordination (strong metal binding energy). In the case of on top adsorption of CH and O, we have considered five data points on each metal ranging from coordination number 4 to coordination number 9 (Figure 3a–e). All the above-mentioned structures were considered for obtaining the linear scaling relations for ΔE_A versus ΔE_M when A = CH or O. It is important to note that the R^2 of the linear scaling relationships approaches unity by introducing more data points. However, we have already shown that these linear scaling relationships hold for various ΔE_A with respect to the α-scheme predicted ΔE_M.[22,26] Nonetheless, the linear scaling relationships derived from this subset of points exhibit a high degree of consistency in agreement with earlier observations.[22] Therefore, it is anticipated that the considered data points would suffice to establish accurate linear scaling relationships between ΔE_A and ΔE_M.

In Figure 4a,b, we summarize the linear scaling relations between the DFT energies ΔE_{CH} and ΔE_O versus ΔE_M, respectively. It is noteworthy to mention that all of the binding energies are with respect to the bulk energy of the considered metal atom. Hence, all binding energies are referenced to the bulk cohesive energy, which corresponds to the simultaneous breaking of 12 bonds per metal atom. This consequently shifts binding energies toward more positive values with coordination, and numbers can become positive for very low metal coordination. The details of the linear relations such as slopes, intercepts and mean absolute errors can be found in Table S2 of the Supporting Information. The observed linear scaling relationships provide strong evidence that ΔE_M serves as an accurate and efficient predictor for ΔE_A. It is important to note that the slopes and intercepts of these linear scaling relationships exhibit specific variations. The values of slopes and intercepts within the linear scaling relationships are contingent upon both the metal's identity and the nature of the adsorbates. In most of the cases, the slopes are negative, which means that increasing site stability ΔE_M leads to a decreasing adsorbate binding ΔE_A and vice versa. These findings align with the results reported in earlier publications.[22] Surprisingly, when examining the case of CH adsorption on the on top site, we find that the slope for ΔE_{CH} versus ΔE_M is positive for the coinage 3d and 4d metals Ag and Cu, almost zero for 3d and

https://doi.org/10.1021/jacsau.4c00759
JACS Au 2024, 4, 4790–4798

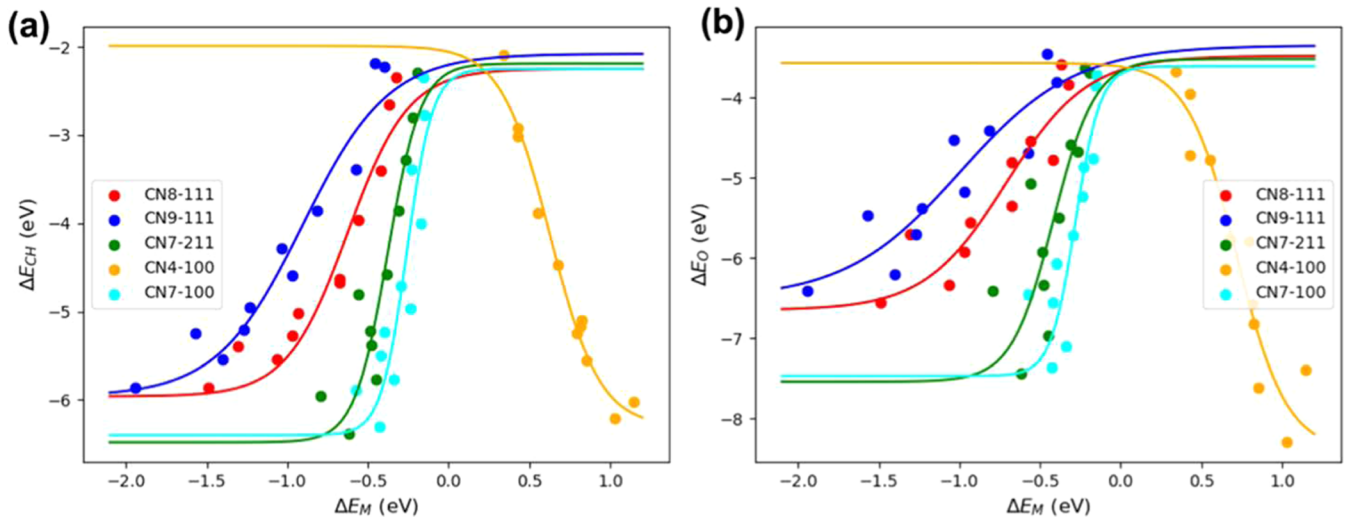

Figure 5. Calculated adsorption energies of (a) ΔE_{CH} and (b) ΔE_O plotted against predicted ΔE_M. The fitting curves show coordination-specific metal-independent correlations for all the considered late transition metals.

4d metals Pd, Ni, Ru, Rh, and Pd, and negative for all of the 5d metals. This observation indicates that the presence of the CH adsorbate leads to a stabilization of the coinage 3d and 4d metals, a near structure independent behavior on the remaining 3d and 4d metals, and strong structure dependence on the 5d metals. In case of O adsorption, only Ag shows a surface stabilizing effect, Cu a near structure independent adsorption, whereas the remaining metals display strong structure dependence.

3.3. Correlation among Various Metals at a Given Coordination Environment

In this section, we study the intricate relationships that exist between adsorption on specific coordination numbers and various transition metals. Our investigation results in a metal-independent correlation among the binding energies of CH and O (ΔE_{CH} and ΔE_O) versus the predicted site stabilities ΔE_M as illustrated in Figure 5. We observe that the adsorption energy ceases to increase further for coordination-specific site stability ΔE_M. Clearly, this is anticipated since energy scaling relations are based on the existence of an optimum electronic density, thus resulting in a maximum binding ΔE_A for a given adsorbate. In this paper, we are focusing primarily on late transition metals, but as we shall see later, the chosen descriptor ΔE_M and its periodicity when filling a single orbital have consequences for the correlations. The cohesive energy of transition metals according to Friedel follows a second-order behavior as a function of d-filling, hence ΔE_M reaches its minimum value when $f_d = 0.5$.[52] Where f_d is the fractional filling of the d-shell. Based on our observations we shall assume that for the late transition metals, the site-dependent correlation among various metals follows a sigmoid function with specific maximum and minimum points. The maximum and minimum adsorption energies strongly depend on the surface site and the specific adsorbate. For a given adsorbate, the range of adsorption energies increases with decreasing coordination of the adsorbed site and the maximum and minimum values can be approximated based on calculated ΔE_A. Based on our observations we shall assume that for the late transition metals the site-dependent correlation among various metals follows a sigmoid function with specific maximum and minimum points. The sigmoid function is the closest to the actual behavior we can get. The more positive the ΔE_M is, the more saturated the bonding with the surface is going to be. In effective medium theory (EMT), one would expect that a maximum saturation is reached when the optimum electronic density (received by the surface) is achieved. In the other extreme when the surface cannot provide electronic states capable of interacting with the adsorbate, the adsorbate is unable to bind to the surface and thus reaches the gas phase level (relative to reference chosen). When fitting the sigmoid function, we have allowed for minimum and maximum values with an absolute variation of 0.10 eV and during the curve fitting the maximum and minimum binding energies are kept fixed within that range for all the considered adsorbates. The sigmoid function is given by the following eq 5

$$\Delta E_A = \Delta E_A^{\min/\max} + (\Delta E_A^{\max/\min} - \Delta E_A^{\min/\max}) /(1 + \exp(-b*(\Delta E_M - c))) \quad (5)$$

$\Delta E_A^{\min}$ and $\Delta E_A^{\max}$ are the maximum and minimum adsorption energies at a specific surface site stability, respectively, b is the rate parameter, and c is descriptor value at the inflection point. Because of the definition of ΔE_M and its strong dependence on coordination number, the c-value in the sigmoid function changes sign, leading to the transition from an s-curve to an inverted s-curve at lower coordination. Interestingly, there should exist an effective coordination number leading to a Heaviside step function with $\left.\frac{\partial \Delta E_A}{\partial \Delta E_M}\right|_{\Delta E_M=0} = \infty$. Given we know the ΔE_M for a given coordination number we can now approximate the adsorption energy ΔE_A from the fitted sigmoid curves. We have listed the parameters for the optimized sigmoid functions for adsorbates CH and O in Table S3 of the Supporting Information.

In addition to exploring the pure metal-based systems, we also investigated the usability of the correlations for alloys. We specifically examined PtPd- and PtIr-based alloys in the case of CN4-100. The model structures are illustrated in Figure S2 of the Supporting Information. We determined the metal binding energies and CH adsorption energies for these systems using DFT calculations. We used the bulk cohesive energy of Pt as a

https://doi.org/10.1021/jacsau.4c00759
JACS Au 2024, 4, 4790−4798

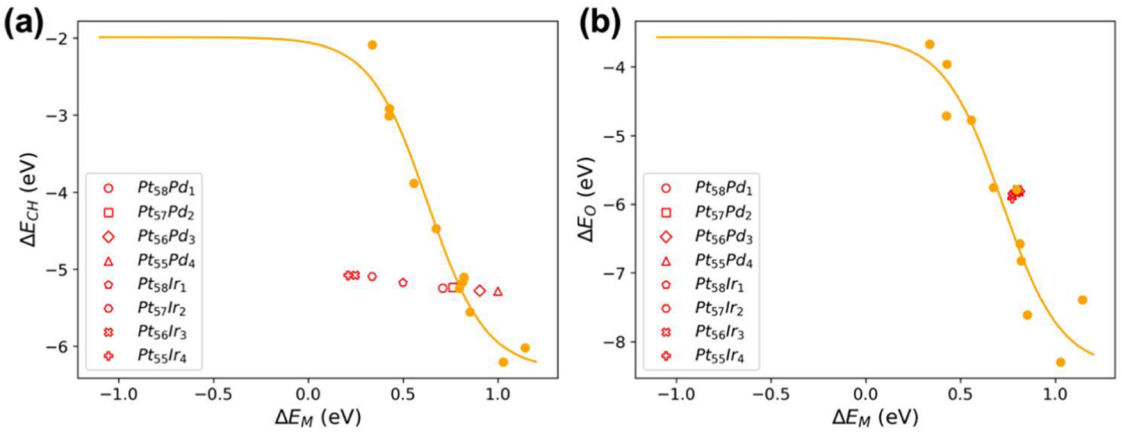

Figure 6. Calculated adsorption energies of (a) ΔE_{CH} plotted against the calculated ΔE_M and (b) calculated adsorption energies of ΔE_O versus predicted ΔE_M where ΔE_M specifically for the alloy systems have been corrected using results from (a). Solid and open symbols are for pure metals and alloy-based systems, respectively. The solid curves represent the metal-independent correlations optimized for the pure metal systems on CN4-100.

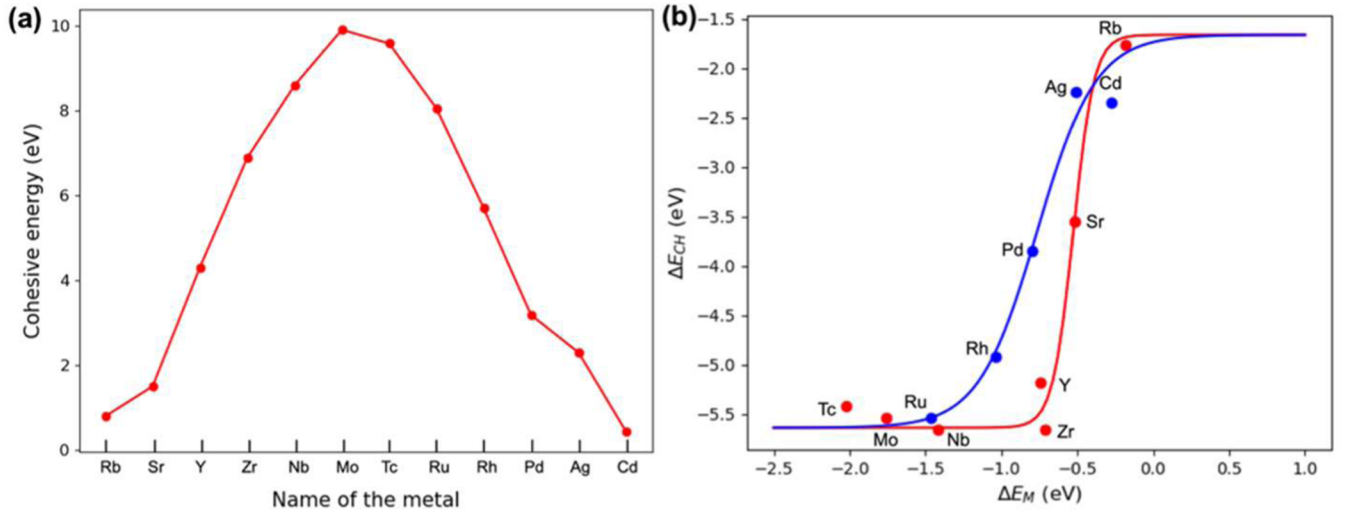

Figure 7. (a) Calculated cohesive energies plotted for 5s and 4d transition metals. (b) Calculated binding energies for on top adsorption of CH, ΔE_{CH}, on close-packed (111) surfaces plotted against the site-specific metal binding energy, ΔE_M, referenced to the bulk cohesive energy of the metal. The solid red curve is best sigmoid fit to metals Rb, Sr, Y, Zr, Nb, Mo, and Tc whereas the blue solid curve is best sigmoid fit to metals Ru, Rh, Pd, Ag, and Cd. All ΔE_M values for these systems have been calculated using DFT.

reference for the metal binding energies. The results are summarized in Figure 6a, and we note that the binding energies of CH on PtPd- and PtIr-based alloys do not follow the same trend found for the pure metal-based systems. Since applying the bulk energy of clean Pt as a reference for the stability of Pt atoms in the alloys is insufficient and no direct DFT calculations can provide such values, to validate our model, we have first extracted the reference metal binding energy in that specific configuration from the best fitted sigmoid function of ΔE_M versus ΔE_{CH}. We then considered the same structures (Figure S2) and the obtained ΔE_M for the prediction of alloy-based O adsorption energies (Figure 6b). With this approach, the O adsorption energies on alloys in the ΔE_M versus ΔE_O plot match well with the pure metal-based sigmoid function (Figure 6b). To summarize, if we know the correct reference of ΔE_M, the metal-independent correlations can be expanded to include alloys and intermetallics, as well.

In this final section, we expand our investigation to include early 4d transition metals and 5s transition metals. Explicitly, we considered Rb, Sr, Y, Zr, Nb, Mo, Tc, Ru, Rh, Pd, Ag, and Cd metals in an fcc crystal structure to obtain a comprehensive understanding of the periodic behavior of adsorption strength versus ΔE_M. We use the on top adsorption of CH on close-packed 111 surfaces (CN9-111) as our model structures and have calculated ΔE_M relative to the bulk metal energies. Because of the periodic trend in the cohesive energies when you fill up the subshell, as shown in Figure 7a, the descriptor ΔE_M will reflect a similar behavior, and the correlation functions introduced cannot be injective for the domain consisting of all metals in the periodic table as seen from Figure 7b. We have divided our correlation of ΔE_{CH} versus ΔE_M into two functions based on the cohesive energy curve in Figure 7a. The range of metals from Rb to Tc follows one sigmoid curve where ΔE_{CH} increases from its minimum to its maximum binding strength and for the range of metals from Ru to Cd where the cohesive energy is decreasing, ΔE_{CH} reverts back to its minimum energy along a different sigmoid curve as shown in Figure 7b. The cyclic behavior of ΔE_{CH} versus ΔE_M for on top adsorption close-packed (111) surface is a consequence of changes in cohesive energy and the bond

https://doi.org/10.1021/jacsau.4c00759
JACS Au 2024, 4, 4790−4798

strength of the adsorbate, where ΔE_M reflects the cohesive energy behavior and the bond strength is related to the d-band characteristics of the metals. A full understanding of this separation into two sigmoid curves and how it depends on the metal−adsorbate interaction would require a more comprehensive study of many different adsorbates with different central bonding elements {C, N, O, S}. However, the behavior is not arbitrary, and it is expected that specific bonding behaviors are recovered when you cycle through the periodic table. The descriptor we are using is closely linked to the changes in the cohesive energy of the metals, and since the cohesive energy is second order in s + d-filling as seen in Figure 7a (Friedel model), we cannot expect an injective mapping describing adsorption energies as a function of our descriptor as seen in Figure 7b. Because of the observed generic behavior, we anticipate a similar cyclic nature for other coordination environments, other metal subshells, and other adsorbates. These insights will provide a valuable tool to better understand the relationship between surface structure and activity and serve as guidance for researchers and engineers in the fields of surface science and catalysis.

Along with the on top adsorption of the CH, we have tested our model for CH hollow adsorption (Figure S3). The predicted ΔE_M values are the average of the considered hollow site. The results show that the predicted ΔE_M show a strong correlation with the ΔE_{CH} at various coordination environments for a specific metal. Moreover, there is a correlation among various metals at specific surface site coordination. Hence, the proposed model can be expanded to various other adsorption sites.

4. CONCLUSIONS

We have investigated the metal independent correlation of ΔE_M versus ΔE_A (A = CH and O) at specific surface site coordination for a range of metals (Ag, Au, Co, Cu, Ir, Ni, Os, Pd, Pt, Rh, and Ru). The coordination-based α-scheme model has been applied to predict ΔE_M, and we have investigated the linear scaling relations between ΔE_M and ΔE_A in various coordination environments. All of the considered metals show strong linear scaling relations between ΔE_A and ΔE_M throughout the considered metal coordination environments. For a specific surface site coordination, ΔE_A shows a correlation with ΔE_M for different metals within a site-specific maximum and minimum energy range. The correlations are best fitted by either sigmoid or reverse sigmoid functions depending on the site coordination, and it suggests that a specific coordination number exists where the correlation is a step function at $\Delta E_M = 0$. In the case of alloy-based system, we considered PtPd- and PtIr-based alloys and investigated the system-independent correlation. In this case, obtaining correct cohesive energies is highly challenging and we explicitly considered one specific system (CH adsorption data) to obtain the correct cohesive energy references. Applying these reference energies to investigate O adsorption data for the same systems we found that the model indeed can be used for alloy and intermetallic systems as well. In addition, we have expanded our model by including data points on early transition metals as well as some s-block elements. Interestingly, the correlation shows cyclic behavior with respect to ΔE_M. This is due to the introduction of the cohesive energy term within ΔE_M which follows second-order behavior as a function of d-filling. Overall, our model enables us to find out the correlation among various metals and alloys at specific surface site coordination. We believe that the model can be expanded further, and because of its versatility can lead to a much broader application.

■ ASSOCIATED CONTENT

Data Availability Statement

A detailed list of DFT energies and structures is provided via the catalysis-hub.org repository[37] at https://www.catalysis-hub.org/publications/MandalMetal2024. The uploaded metal binding energies are with respect to the gas phase metal energies. To get the metal binding energies with respect to bulk, we just need to add 2.3315, 2.8379, 6.2614, 3.2219, 8.2122, 4.8444, 10.2433, 3.2039, 5.3803, 5.7123, 8.0630, 0.7979, 1.5048, 4.3132, 6.8903, 8.6009, 9.9139, 9.5918, and 0.4430 eV for Ag, Au, Co, Cu, Ir, Ni, Os, Pd, Pt, Rh, Ru, Rb, Sr, Y, Zr, Nb, Mo, Tc, and Cd metals, respectively.

Supporting Information

The Supporting Information is available free of charge at https://pubs.acs.org/doi/10.1021/jacsau.4c00759.

The α_i^Z values of considered metals including corrections for subsurface, comparison of the α-scheme model-predicted and DFT-calculated ΔE_M, linear fitting parameters along with mean absolute errors of ΔE_A versus ΔE_M for all the considered metals where adsorbates are CH and O, sigmoid fitting equations at a specific surface site stability for various metals using predicted ΔE_M versus DFT-calculated ΔE_{CH} and ΔE_O, considered PtPd- and PtIr alloy-based structures at CN4-100, structures for CH hollow adsorption, plot against ΔE_{CH} and ΔE_M, and coordination-specific metal-independent correlations (PDF)

■ AUTHOR INFORMATION

Corresponding Author

Frank Abild-Pedersen − *SUNCAT Center for Interface Science and Catalysis, SLAC National Accelerator Laboratory, Menlo Park, California 94025, United States;* orcid.org/0000-0002-1911-074X; Email: abild@slac.stanford.edu

Author

Shyama Charan Mandal − *SUNCAT Center for Interface Science and Catalysis, Department of Chemical Engineering, Stanford University, Stanford, California 94305, United States; SUNCAT Center for Interface Science and Catalysis, SLAC National Accelerator Laboratory, Menlo Park, California 94025, United States*

Complete contact information is available at: https://pubs.acs.org/10.1021/jacsau.4c00759

Notes

The authors declare no competing financial interest.

■ ACKNOWLEDGMENTS

We acknowledge support from the U.S. Department of Energy, Office of Science, Office of Basic Energy Sciences, Chemical Sciences, Geosciences, and Biosciences Division, Catalysis Science Program to the SUNCAT Center for Interface Science and Catalysis. This research used resources of the National Energy Research Scientific Computing Center; a DOE Office

https://doi.org/10.1021/jacsau.4c00759
JACS Au 2024, 4, 4790−4798

of Science User Facility supported by the Office of Science of the U.S. Department of Energy under Contract No. DE-AC02-05CH11231 using NERSC award BES-ERCAP0024127. We acknowledge computational support from the SLAC Scientific Data Facility (SDF).

REFERENCES

(1) Savignan, L.; Faucher, S.; Chéry, P.; Lespes, G. Platinum Group Elements Contamination in Soils: Review of the Current State. *Chemosphere* **2021**, *271*, No. 129517.
(2) McCrory, C. C. L.; Jung, S.; Ferrer, I. M.; Chatman, S. M.; Peters, J. C.; Jaramillo, T. F. Benchmarking Hydrogen Evolving Reaction and Oxygen Evolving Reaction Electrocatalysts for Solar Water Splitting Devices. *J. Am. Chem. Soc.* **2015**, *137* (13), 4347−4357.
(3) Nørskov, J. K.; Rossmeisl, J.; Logadottir, A.; Lindqvist, L.; Kitchin, J. R.; Bligaard, T.; Jónsson, H. Origin of the Overpotential for Oxygen Reduction at a Fuel-Cell Cathode. *J. Phys. Chem. B* **2004**, *108* (46), 17886−17892.
(4) Hao, H.; Jin, B.; Liu, W.; Wu, X.; Yin, F.; Liu, S. Robust Pt@TiO_x/TiO_2 Catalysts for Hydrocarbon Combustion: Effects of Pt-TiO_x Interaction and Sulfates. *ACS Catal.* **2020**, *10* (22), 13543−13548.
(5) Kamat, G. A.; Zamora Zeledón, J. A.; Gunasooriya, G. T. K. K.; Dull, S. M.; Perryman, J. T.; Nørskov, J. K.; Stevens, M. B.; Jaramillo, T. F. Acid Anion Electrolyte Effects on Platinum for Oxygen and Hydrogen Electrocatalysis. *Commun. Chem.* **2022**, *5* (1), 20.
(6) Zhang, C.; Shen, X.; Pan, Y.; Peng, Z. A Review of Pt-Based Electrocatalysts for Oxygen Reduction Reaction. *Front. Energy* **2017**, *11* (3), 268−285.
(7) Hansen, J. N.; Prats, H.; Toudahl, K. K.; Mørch Secher, N.; Chan, K.; Kibsgaard, J.; Chorkendorff, I. Is There Anything Better than Pt for HER? *ACS Energy Lett.* **2021**, *6* (4), 1175−1180.
(8) Hughes, A. E.; Haque, N.; Northey, S. A.; Giddey, S. Platinum Group Metals: A Review of Resources, Production and Usage with a Focus on Catalysts. *Resources* **2021**, *10* (9), 93.
(9) Yang, A.-C.; Choksi, T.; Streibel, V.; Aljama, H.; Wrasman, C. J.; Roling, L. T.; Goodman, E. D.; Thomas, D.; Bare, S. R.; Sánchez-Carrera, R. S.; Schäfer, A.; Li, Y.; Abild-Pedersen, F.; Cargnello, M. Revealing the Structure of a Catalytic Combustion Active-Site Ensemble Combining Uniform Nanocrystal Catalysts and Theory Insights. *Proc. Natl. Acad. Sci. U.S.A.* **2020**, *117* (26), 14721−14729.
(10) Yang, A.-C.; Streibel, V.; Choksi, T. S.; Aljama, H.; Werghi, B.; Bare, S. R.; Sánchez-Carrera, R. S.; Schäfer, A.; Li, Y.; Abild-Pedersen, F.; Cargnello, M. Insights and Comparison of Structure−Property Relationships in Propane and Propene Catalytic Combustion on Pd- and Pt-Based Catalysts. *J. Catal.* **2021**, *401*, 89−101.
(11) Dahl, S.; Logadottir, A.; Egeberg, R. C.; Larsen, J. H.; Chorkendorff, I.; Törnqvist, E.; Nørskov, J. K. Role of Steps in N_2 Activation on Ru(0001). *Phys. Rev. Lett.* **1999**, *83* (9), 1814−1817.
(12) Greeley, J.; Mavrikakis, M. Alloy Catalysts Designed from First Principles. *Nat. Mater.* **2004**, *3* (11), 810−815.
(13) Tripa, C. E.; Zubkov, T. S.; Yates, J. T.; Mavrikakis, M.; Nørskov, J. K. Molecular N_2 Chemisorption—Specific Adsorption on Step Defect Sites on Pt Surfaces. *J. Chem. Phys.* **1999**, *111* (18), 8651−8658.
(14) Abild-Pedersen, F. Computational Catalyst Screening: Scaling, Bond-Order and Catalysis. *Catal. Today* **2016**, *272*, 6−13.
(15) Ma, Z.; Cano, Z. P.; Yu, A.; Chen, Z.; Jiang, G.; Fu, X.; Yang, L.; Wu, T.; Bai, Z.; Lu, J. Enhancing Oxygen Reduction Activity of Pt-Based Electrocatalysts: From Theoretical Mechanisms to Practical Methods. *Angew. Chem., Int. Ed.* **2020**, *59* (42), 18334−18348.
(16) Marei, M. N.; Khan, H. A.; Badra, J. A.; Montoya, A.; Farooq, A.; Masri, A. R. Comparative Study of the Catalytic Oxidation of Hydrocarbons on Platinum and Palladium Wires and Nanoparticles. *Energy Fuels* **2022**, *36* (4), 2044−2057.
(17) Shi, X.; Lin, X.; Luo, R.; Wu, S.; Li, L.; Zhao, Z.-J.; Gong, J. Dynamics of Heterogeneous Catalytic Processes at Operando Conditions. *JACS Au* **2021**, *1* (12), 2100−2120.
(18) Toyao, T.; Maeno, Z.; Takakusagi, S.; Kamachi, T.; Takigawa, I.; Shimizu, K. Machine Learning for Catalysis Informatics: Recent Applications and Prospects. *ACS Catal.* **2020**, *10* (3), 2260−2297.
(19) Ma, X.; Xin, H. Orbitalwise Coordination Number for Predicting Adsorption Properties of Metal Nanocatalysts. *Phys. Rev. Lett.* **2017**, *118* (3), No. 036101.
(20) Calle-Vallejo, F.; Tymoczko, J.; Colic, V.; Vu, Q. H.; Pohl, M. D.; Morgenstern, K.; Loffreda, D.; Sautet, P.; Schuhmann, W.; Bandarenka, A. S. Finding Optimal Surface Sites on Heterogeneous Catalysts by Counting Nearest Neighbors. *Science* **2015**, *350* (6257), 185−189.
(21) Abild-Pedersen, F.; Greeley, J.; Studt, F.; Rossmeisl, J.; Munter, T. R.; Moses, P. G.; Skúlason, E.; Bligaard, T.; Nørskov, J. K. Scaling Properties of Adsorption Energies for Hydrogen-Containing Molecules on Transition-Metal Surfaces. *Phys. Rev. Lett.* **2007**, *99* (1), No. 016105.
(22) Mandal, S. C.; Abild-Pedersen, F. Classification of Adsorbed Hydrocarbons Based on Bonding Configurations of the Adsorbates and Surface Site Stabilities. *ACS Catal.* **2023**, *13* (20), 13663−13671.
(23) Mamun, O.; Winther, K. T.; Boes, J. R.; Bligaard, T. A Bayesian Framework for Adsorption Energy Prediction on Bimetallic Alloy Catalysts. *Npj Comput. Mater.* **2020**, *6* (1), 177.
(24) Roling, L. T.; Li, L.; Abild-Pedersen, F. Configurational Energies of Nanoparticles Based on Metal−Metal Coordination. *J. Phys. Chem. C* **2017**, *121* (41), 23002−23010.
(25) Saini, S.; Halldin Stenlid, J.; Deo, S.; Plessow, P. N.; Abild-Pedersen, F. A First-Principles Approach to Modeling Surface Site Stabilities on Multimetallic Catalysts. *ACS Catal.* **2024**, *14* (2), 874−885.
(26) Roling, L. T.; Abild-Pedersen, F. Structure-Sensitive Scaling Relations: Adsorption Energies from Surface Site Stability. *ChemCatChem.* **2018**, *10* (7), 1643−1650.
(27) Kulkarni, A.; Siahrostami, S.; Patel, A.; Nørskov, J. K. Understanding Catalytic Activity Trends in the Oxygen Reduction Reaction. *Chem. Rev.* **2018**, *118* (5), 2302−2312.
(28) Kresse, G.; Hafner, J. *Ab Initio* Molecular Dynamics for Liquid Metals. *Phys. Rev. B* **1993**, *47* (1), 558−561.
(29) Kresse, G.; Furthmüller, J. Efficiency of Ab-Initio Total Energy Calculations for Metals and Semiconductors Using a Plane-Wave Basis Set. *Comput. Mater. Sci.* **1996**, *6* (1), 15−50.
(30) Kresse, G.; Furthmüller, J. Efficient Iterative Schemes for *Ab Initio* Total-Energy Calculations Using a Plane-Wave Basis Set. *Phys. Rev. B* **1996**, *54* (16), 11169−11186.
(31) Hjorth Larsen, A.; Jørgen Mortensen, J.; Blomqvist, J.; Castelli, I. E.; Christensen, R.; Dułak, M.; Friis, J.; Groves, M. N.; Hammer, B.; Hargus, C.; Hermes, E. D.; Jennings, P. C.; Bjerre Jensen, P.; Kermode, J.; Kitchin, J. R.; Leonhard Kolsbjerg, E.; Kubal, J.; Kaasbjerg, K.; Lysgaard, S.; Bergmann Maronsson, J.; Maxson, T.; Olsen, T.; Pastewka, L.; Peterson, A.; Rostgaard, C.; Schiøtz, J.; Schütt, O.; Strange, M.; Thygesen, K. S.; Vegge, T.; Vilhelmsen, L.; Walter, M.; Zeng, Z.; Jacobsen, K. W. The Atomic Simulation Environment—A Python Library for Working with Atoms. *J. Phys.: Condens. Matter* **2017**, *29* (27), No. 273002.
(32) Wellendorff, J.; Lundgaard, K. T.; Møgelhøj, A.; Petzold, V.; Landis, D. D.; Nørskov, J. K.; Bligaard, T.; Jacobsen, K. W. Density Functionals for Surface Science: Exchange-Correlation Model Development with Bayesian Error Estimation. *Phys. Rev. B* **2012**, *85* (23), No. 235149.
(33) Lee, K.; Murray, É. D.; Kong, L.; Lundqvist, B. I.; Langreth, D. C. Higher-Accuracy van der Waals Density Functional. *Phys. Rev. B* **2010**, *82* (8), No. 081101.
(34) Tahsini, N.; Yang, A.-C.; Streibel, V.; Werghi, B.; Goodman, E. D.; Aitbekova, A.; Bare, S. R.; Li, Y.; Abild-Pedersen, F.; Cargnello, M. Colloidal Platinum−Copper Nanocrystal Alloy Catalysts Surpass Platinum in Low-Temperature Propene Combustion. *J. Am. Chem. Soc.* **2022**, *144* (4), 1612−1621.

https://doi.org/10.1021/jacsau.4c00759
JACS Au 2024, 4, 4790−4798

(35) Monkhorst, H. J.; Pack, J. D. Special Points for Brillouin-Zone Integrations. *Phys. Rev. B* **1976**, *13* (12), 5188−5192.
(36) Bengtsson, L. Dipole Correction for Surface Supercell Calculations. *Phys. Rev. B* **1999**, *59* (19), 12301−12304.
(37) Winther, K. T.; Hoffmann, M. J.; Boes, J. R.; Mamun, O.; Bajdich, M.; Bligaard, T. Catalysis-Hub.Org, An Open Electronic Structure Database for Surface Reactions. *Sci. Data* **2019**, *6* (1), 75.
(38) Yang, H.; Whitten, J. L. Dissociative Adsorption of H_2 on Ni(111). *J. Chem. Phys.* **1993**, *98* (6), 5039−5049.
(39) Aireddy, D. R.; Ding, K. Heterolytic Dissociation of H_2 in Heterogeneous Catalysis. *ACS Catal.* **2022**, *12* (8), 4707−4723.
(40) Fang, H.; Wu, S.; Ayvali, T.; Zheng, J.; Fellowes, J.; Ho, P.-L.; Leung, K. C.; Large, A.; Held, G.; Kato, R.; Suenaga, K.; Reyes, Y. I. A.; Thang, H. V.; Chen, H.-Y. T.; Tsang, S. C. E. Dispersed Surface Ru Ensembles on MgO(111) for Catalytic Ammonia Decomposition. *Nat. Commun.* **2023**, *14* (1), No. 647.
(41) Cushing, G. W.; Navin, J. K.; Donald, S. B.; Valadez, L.; Johánek, V.; Harrison, I. C−H Bond Activation of Light Alkanes on Pt(111): Dissociative Sticking Coefficients, Evans−Polanyi Relation, and Gas−Surface Energy Transfer. *J. Phys. Chem. C* **2010**, *114* (40), 17222−17232.
(42) Latimer, A. A.; Kulkarni, A. R.; Aljama, H.; Montoya, J. H.; Yoo, J. S.; Tsai, C.; Abild-Pedersen, F.; Studt, F.; Nørskov, J. K. Understanding Trends in C−H Bond Activation in Heterogeneous Catalysis. *Nat. Mater.* **2017**, *16* (2), 225−229.
(43) Santoro, S.; Kozhushkov, S. I.; Ackermann, L.; Vaccaro, L. Heterogeneous Catalytic Approaches in C−H Activation Reactions. *Green Chem.* **2016**, *18* (12), 3471−3493.
(44) Ferriday, T. B.; Middleton, P. H.; Kolhe, M. L. Review of the Hydrogen Evolution Reaction—A Basic Approach. *Energies* **2021**, *14* (24), 8535.
(45) Yu, J.; Qin, X.; Yang, Y.; Lv, M.; Yin, P.; Wang, L.; Ren, Z.; Song, B.; Li, Q.; Zheng, L.; Hong, S.; Xing, X.; Ma, D.; Wei, M.; Duan, X. Highly Stable Pt/CeO_2 Catalyst with Embedding Structure toward Water−Gas Shift Reaction. *J. Am. Chem. Soc.* **2024**, *146* (1), 1071−1080.
(46) Shao, M.; Chang, Q.; Dodelet, J.-P.; Chenitz, R. Recent Advances in Electrocatalysts for Oxygen Reduction Reaction. *Chem. Rev.* **2016**, *116* (6), 3594−3657.
(47) Huang, L.; Zaman, S.; Tian, X.; Wang, Z.; Fang, W.; Xia, B. Y. Advanced Platinum-Based Oxygen Reduction Electrocatalysts for Fuel Cells. *Acc. Chem. Res.* **2021**, *54* (2), 311−322.
(48) Daiane Ferreira Da Silva, C.; Claudel, F.; Martin, V.; Chattot, R.; Abbou, S.; Kumar, K.; Jiménez-Morales, I.; Cavaliere, S.; Jones, D.; Rozière, J.; Solà-Hernandez, L.; Beauger, C.; Faustini, M.; Peron, J.; Gilles, B.; Encinas, T.; Piccolo, L.; Barros De Lima, F. H.; Dubau, L.; Maillard, F. Oxygen Evolution Reaction Activity and Stability Benchmarks for Supported and Unsupported IrO_x Electrocatalysts. *ACS Catal.* **2021**, *11* (7), 4107−4116.
(49) Wu, H.; Wang, Y.; Shi, Z.; Wang, X.; Yang, J.; Xiao, M.; Ge, J.; Xing, W.; Liu, C. Recent Developments of Iridium-Based Catalysts for the Oxygen Evolution Reaction in Acidic Water Electrolysis. *J. Mater. Chem. A* **2022**, *10* (25), 13170−13189.
(50) Mandal, S. C.; Das, A.; Roy, D.; Das, S.; Nair, A. S.; Pathak, B. Developments of the Heterogeneous and Homogeneous CO_2 Hydrogenation to Value-Added C_{2+}-Based Hydrocarbons and Oxygenated Products. *Coord. Chem. Rev.* **2022**, *471*, No. 214737.
(51) Peng, H.-J.; Tang, M. T.; Halldin Stenlid, J.; Liu, X.; Abild-Pedersen, F. Trends in Oxygenate/Hydrocarbon Selectivity for Electrochemical CO(2) Reduction to C_2 Products. *Nat. Commun.* **2022**, *13* (1), No. 1399.
(52) Friedel, J. *The Physics of Metals*; Cambridge University Press: London, 1969.

https://doi.org/10.1021/jacsau.4c00759
JACS Au 2024, 4, 4790−4798